Improved Few-Group Coarse-Mesh Method for Calculating Three-Dimensional Power Distribution in Fast Breeder Reactor

by

Yasuo Komano, Toshikazu Takeda, Tamotsu Sekiya

Department of Nuclear Engineering, Faculty of Engineering,
Osaka University

Abstract

An effective few-group coarse mesh method has been developed for calculating three-dimensional power distribution in fast breeder reactors by extending Askew's one-group coarse mesh method. This method uses modified macroscopic cross sections including group-dependent corrections for coarse meshes of one point per hexagon in each radial plane and can be easily incorporated into conventional diffusion codes.

Results obtained in few-group three-dimensional test cases on a prototype fast breeder reactor show that this method is as accurate as fine mesh calculations with six mesh points per hexagon, and the computing time is about 1/8 of that of fine mesh calculations.

I. Introduction

A lot of problems associated with nuclear designs of fast breeder reactors require three-dimensional (3-D) representation of the cores. The multi-group fine mesh 3-D diffusion calculation, however, consumes a large and often prohibitive amount of computer time. On the other hand conventional coarse mesh calculations yield a maximum error of about 10% in power distribution. Therefore it is desirable to develop a technique which solves the diffusion equation using coarse meshes with comparable accuracy to fine mesh calculations.

Finneman and Wagner[1] developed a new computational technique (nodal expansion method) for the solution of multi-dimensional diffusion problems. The nodal expansion method yields accurate results using coarse meshes, but it requires an additional fine mesh 1-D calculation to the multi-dimensional calculation. If we want to apply this method to the conventional diffusion codes, we have to add a new calculating routine for the coupling coefficient. This makes it troublesome to incorporate the nodal expansion method into the diffusion codes. Suzuki[2] developed a similar coarse mesh method for LMFBR's. His method, however , treats the coarse mesh effect only for control rods, and hence further improvement is necessary for correcting the coarse mesh error of about 5% in the power distribution in core regions.

Askew et al.[3] developed an ingenious one-group coarse mesh correction method in which supplementary mesh points

are added to coarse mesh points. This method is very simple and effective for the coarse mesh correction. However it is in the framework of one-group theory and also requires a considerable change in the calculating algorithm for the finite difference equation.

We have developed an improved few-group coarse mesh method by modifying Askew's one-group method to incorporate easily into conventional diffusion codes such as CITATION[4] and GAUGE [5]. This method employs modified macroscopic cross sections including group-dependent corrections for coarse meshes. On the basis of this method we have made a few-group 3-D diffusion code ICOM. The calculational accuracy of the ICOM code has been tested on a sodium-cooled prototype fast reactor "MONJU" by comparing the results with those obtained by 3-D few-group fine mesh calculations.

II. Improved Few-Group Coarse Mesh Method

We introduce an improved few-group coarse mesh method in 3-D system. Figure 1 represents a 3-D hexagonal-Z geometry in which points B_i are centers of the assemblies i (i=0~8) and h_r and h_{iz} are mesh intervals along radial and axial directions. Askew added supplementary mesh points A_{ij} and A_{ji} by dividing the mesh intervals, h_r and h_{iz}, between the two centers into three parts of equal length. Neutron fluxes in group g at the points B_i, A_{ij} and A_{ji} are devoted by ϕ^g_{Bi}, ϕ^g_{Aij} and ϕ^g_{Aji}, respectively.

In the conventional coarse mesh calculation in which mesh points are B_i, the net neutron current through the interface S_{0r} between the assemblies 0 and 1 is given by

$$J^g_c = -\left[\frac{2D^g_0 D^g_1 S_{0r}}{h_r(D^g_0 + D^g_1)}\right](\phi^g_{B1} - \phi^g_{B0}) \quad , \qquad (1)$$

where D^g_i is the diffusion coefficient of assembly i in group g. Equation (1) yields a relatively large error because of the large mesh interval h_r. To reduce this error, Askew used the fluxes at the supplementary points A_{ij} and A_{ji} in calculating the net neutron current. This procedure leads to the following net current through the interface S_{0r}:

$$J^g_f = -\left[\frac{6D^g_0 D^g_1 S_{0r}}{h_r(D^g_0 + D^g_1)}\right](\phi^g_{A10} - \phi^g_{A01}) \qquad (2)$$

To represent J_f^g in terms of ϕ_{Bo}^g and ϕ_{B1}^g, neutron balance relations in regions R_0 and R_1 (see Fig.1) are used. Net incoming neutron currents in group g through the right and left interfaces of region R_0 are expressed by $D_0^g(\phi_{Bo}^g - \phi_{Ao1}^g)/(h_r/3)$ and $2D_0^gD_1^g(\phi_{Ao}^g - \phi_{Ao1}^g)/\left[(D_0^g+D_1^g)h_r/3\right]$, respectively, and those of region R_1 are expressed by $2D_0^gD_1^g(\phi_{Ao1}^g - \phi_{Ao}^g)/\left[(D_1^g+D_0^g)h_r/3\right]$ and $D_1^g(\phi_{B1}^g - \phi_{Ao}^g)/(h_r/3)$, respectively. Then the neutron balance relation over region R_0 is

$$\frac{D_0^g(\phi_{Bo}^g - \phi_{Ao1}^g)}{h_r/3} + \frac{2D_0^gD_1^g(\phi_{Ao}^g - \phi_{Ao1}^g)}{(D_0^g+D_1^g)h_r/3} + \frac{h_r}{3}D_0^g\beta_{0g}^2\phi_{Ao1}^g = 0 \quad , \tag{3}$$

and that over region R_1 is

$$\frac{D_1^g(\phi_{B1}^g - \phi_{Ao}^g)}{h_r/3} + \frac{2D_1^gD_0^g(\phi_{Ao1}^g - \phi_{Ao}^g)}{(D_1^g+D_0^g)h_r/3} + \frac{h_r}{3}D_1^g\beta_{1g}^2\phi_{Ao}^g = 0 \quad , \tag{4}$$

where

$$\beta_{ig}^2 = \frac{1}{D_i^g}\left[\frac{\chi^g}{K_{eff}}\sum_{g'}\nu\Sigma_{fi}^{g'}\frac{\phi_{Aij}^{g'}}{\phi_{Aij}^g} + \sum_{g'\neq g}\Sigma_{si}^{g'\to g}\frac{\phi_{Aij}^{g'}}{\phi_{Aij}^g} - \Sigma_{ai}^g - \Sigma_{ri}^g\right] \quad , \tag{5}$$

$\nu\Sigma_{fi}^g$: Neutron production cross section in group g of assembly i

χ^g : Normalized neutron fission spectrum in group g

$\Sigma_{si}^{g'\to g}$: Scattering cross section from group g' to g of assembly i

$\Sigma_{ai}^g, \Sigma_{ri}^g$: Absorption and removal cross sections in group g of assembly i

K_{eff} : Neutron multiplication factor .

It should be noted here that, in one-group problems treated by Askew, β_{ig}^2 reduces to $(\nu\Sigma_{fi}/K_{eff}-\Sigma_{ai})/D_i$ and does not depend on the fluxes ϕ_{Aij}^g. Using Eqs. (3) and (4), Eq. (2) can be written as follows:

$$J_f^g = -\left[\frac{2D_{or}^{g*}D_{ir}^{g*}S_{or}}{h_r(D_{or}^{g*}+D_{ir}^{g*})}\right]\left(\phi_{B_1}^{g*}-\phi_{B_o}^{g*}\right), \tag{6}$$

where

$$D_{ir}^{g*} = D_i^g\left(1-\frac{2}{27}h_r^2\beta_{ig}^2\right), \tag{7}$$

$$\phi_{Bi}^{g*} = \phi_{Bi}^g \Big/ \left(1-\frac{1}{q}h_r^2\beta_{ig}^2\right) \tag{8}$$

Use of Eq. (5) and similar expressions for leakage rates through upper and lower boundaries of assembly 0 leads to the following neutron balance equation in assembly:

$$\sum_{i=1}^{6}\left[-\frac{2D_{ir}^{g*}D_{or}^{g*}S_{or}}{h_r(D_{ir}^{g*}+D_{or}^{g*})}\right]\left(\frac{\phi_{Bi}^g}{1-\frac{1}{q}h_r^2\beta_{ig}^2}-\frac{\phi_{Bo}^g}{1-\frac{1}{q}h_r^2\beta_{ig}^2}\right)$$

$$+\sum_{i=7}^{8}\left[-\frac{2D_{oz}^{g*}D_{iz}^{g*}S_z}{h_{oz}D_{iz}^{g*}+h_{iz}D_{oz}^{g*}}\right]\left(\frac{\phi_{Bi}^g}{1-\frac{1}{q}h_{iz}^2\beta_{ig}^2}-\frac{\phi_{Bo}^g}{1-\frac{1}{q}h_{oz}^2\beta_{og}^2}\right)$$

$$+\Sigma_{ao}^g\phi_{Bo}^gV_o+\Sigma_{ro}^g\phi_{Bo}^gV_o=\frac{\chi^g}{K_{eff}}\sum_{g'}\nu\Sigma_{fo}^{g'}\phi_{Bo}^{g'}V_o+\sum_{g'\neq g}\Sigma_{so}^{g'\to g}\phi_{Bo}^{g'}V_o, \tag{9}$$

where

$$D_{iz}^{g*} = D_i^g\left(1-\frac{2}{27}h_{iz}^2\beta_{ig}^2\right) \tag{10}$$

The first and second terms represent neutron leakage rates through six side boundaries and the two upper and lower boundaries, and V_o is the volume of assembly 0. Equation (9) is an extention of Askew's method to few-group problems, but it has a form different from the finite difference equation of the conventional diffusion theory. Therefore a considerable change is necessary for the calculating algolithm of the finite difference equation to incorporate the Askew's method to conventional diffusion codes. Then we develop a modified coarse mesh method which can be easily incorporated into conventional diffusion codes by transforming Eq. (9).

Substitution of ϕ_{Bo}^{g*} for ϕ_{Bo}^{g} in Eq. (9) gives the following equation:

$$\sum_{i=1}^{6}\left[-\frac{2D_{ir}^{g*}D_{or}^{g*}S_{or}}{h_r(D_{ir}^{g*}+D_{or}^{g*})}\left(\phi_{Bi}^{g*}-\phi_{Bo}^{g*}\right)\right]+\sum_{i=7}^{8}\left[-\frac{2D_{oz}^{g*}D_{iz}^{g*}S_z}{h_{oz}D_{iz}^{g*}+h_{iz}D_{oz}^{g*}}\left(\gamma_i^g\phi_{Bi}^{g*}-\gamma_o^g\phi_{Bo}^{g*}\right)\right]$$
$$+\Sigma_{ao}^{g*}\phi_{Bo}^{g*}V_o+\Sigma_{ro}^{g*}\phi_{Bo}^{g*}V_o=\frac{\chi^g}{K_{eff}}\sum_{g'}\nu\Sigma_{fo}^{g'*}\phi_{Bo}^{g'*}V_o+\sum_{g'\to g}\Sigma_{so}^{g'\to g*}\phi_{Bo}^{g'*}V_o, \qquad (11)$$

where

$$\Sigma_{xi}^{g*}=\Sigma_{xi}^{g}\left(1-\frac{1}{q}h_r^2\beta_{ig}^2\right)\quad[x=a,r,s,f], \qquad (12)$$

$$\gamma_i^g=\left(1-\frac{1}{q}h_r^2\beta_{ig}^2\right)\Big/\left(1-\frac{1}{q}h_{iz}^2\beta_{ig}^2\right). \qquad (13)$$

Equation (11) is similar to the expression of the conventional coarse mesh finite difference equation. In the expression, however, D_i^{g*}, Σ_{ai}^{g*}, $\nu\Sigma_{fi}^{g*}$ and ϕ_i^{g*} are substituted for D_i^g, Σ_{ai}^g, $\nu\Sigma_{fi}^g$ and ϕ_i^g, respectively, and γ_i^g is used in expressing axial leakage rates. Therefore the error due to coarse mesh can be reduced by the use of the modified cross sections defined by Eq. (12) and the modified diffusion coefficients by Eqs. (7) and (10) in the conventional few-group coarse mesh finite difference equation.

Here it should be noted that these modified cross sections depend on the fluxes at supplementary mesh points which cannot be evaluated by the coarse mesh calculation. Then we approximate the flux ratio $\phi_{Aij}^{g'} / \phi_{Aij}^g$ in Eq. (5) by the ratio $\phi_{Bi}^{g'} / \phi_{Bi}^g$ which can be calculated by the coarse mesh calculation. Thus, in the improved coarse mesh calculation, we have to recalculate the modified cross sections for each outer iteration using resultant fluxes and K_{eff}.

Figure 2 shows the calculational flow of the improved coarse mesh method. The calculation of the modified cross sections needs a computing time as much as that of the inner iteration, so the usual inner and outer iterations are repeated first until K_{eff} and the neutron flux are converged in order to save the computing time.

III. Numerucal Results and Discussions

This chapter describes results of the test calculations for the improved few-group coarse mesh calculation on a 300 MWe prototype fast breeder reactor "MONJU" shown in Fig. 3. The reactor consists of inner core, outer core, blanket and nineteen control rod channels. Calculations are performed in three-group model using the macroscopic cross sections for an equilibrium core shown in Table 1. Three control rod patterns (A, B, C) were treated; all the control rods are withdrawn for the pattern A, twelve control rods installed at the 5th and 6th rows are half inserted for the pattern B and the twelve control rods are fully inserted for the pattern C.

Table 2 shows the multiplication factors and the control-rod-worth obtained by the three methods; fine mesh calculation, conventional and improved coarse mesh calculations. The improved coarse mesh calculation gives values of K_{eff} which agree with those obtained by the fine mesh calculation within 0.1%, while the conventional coarse mesh calculation yields a maximum relative error of 1.1% in K_{eff}. The errors in the control-rod-worths obtained by the present coarse mesh calculations are only about 1% relative to the results of the fine mesh calculations, and are far less than those of 10% by the conventional coarse mesh calculations. Figures 4(a),(b) and (c) show the convergence processes of K_{eff} for three calculations as a function of the number of outer iterations for the patterns A, B and C, respectively. A remarkable improvement of K_{eff} can be seen with the use of the coarse

mesh correction.

Table 3 shows the power fractions in each region obtained with the three calculations. The power fraction obtained with the conventional coarse mesh calculation agrees with that with the fine mesh calculation within 0.6% for every region. The conventional coarse mesh calculation gives relative errors of 1.8% in the outer core and of 4.5% in the blanket.

Figure 5 shows power density (watt/cc) and percent error in power density for the conventional and the present coarse mesh calculations relative to the fine mesh calculation; (a) shows results on a central radial plane and (b) shows those on a radial plane adjacent to upper blanket, respectively, for the pattern B. The values are shown only for 1/6 of the core because of its symmetry. The conventional coarse mesh calculation yields maximum errors in the power distribution of about 3% at the core center, and of about 9% in the first row of the blanket. On the other hand the maximum error of the present method is about 1% for all the regions. Figures 6(a) and (b) show percent errors in each of the three-group fluxes on a central plane obtained by the conventional and the improved coarse mesh calculations, respectively. In the conventional coarse mesh calculation (Fig. 6(a)), the fluxes at the control-rod channel are underestimated by about 10% for each group. In the present calculation (Fig. 6(b)), the fluxes at that channel are remarkably improved.

The correction factors for the macroscopic cross sections used in the present coarse mesh calculation for the pattern B, $(1-(1/9)h_r^2\beta_{ig}^2)$, are given in Fig. 7 for the three energy-

groups on a central plane. It should be noticed that this factor becomes about 1.1 on the control-rod channels, resulting in the improvement of the fluxes in the control-rod channel, and the value in the blanket region depends strongly on energy-group.

Figures 8(a), (b) and (c) show 1st-group, 2nd-group and 3rd-group axial flux distributions for the three methods at the control-rod channel, respectively. The axial group-flux distributions along the fuel assembly at the core center are shown in Fig. 9. It is seen that the axial flux distributions obtained by the present method well agree with those by the fine mesh calculation.

Table 4 represents the computing times needed for the fine mesh calculation, and the present and the conventional coarse mesh calculations. The present coarse mesh calculation is about 8 times faster than the fine mesh calculation based on the CITATION code and the increase in the computing time is only 50% relative to the conventional coarse mesh calculation.

IV. Conclusion

An improved few-group coarse mesh method based on Askew's method has been developed for calculating the power distribution of fast reactors in a 3-D, hexagonal-Z core model.

Concerning the numerical results of the power distribution given by this code, the deviation from the value based on the fine mesh calculation remains only about 1% for all the regions, while the conventional coarse mesh calculation yields a maximum deviation of about 3% in the core, and of about 9% in the blanket. The calculation based on the present improved coarse mesh method needs the CPU time which is 8 times smaller than the fine mesh calculation.

Acknowledgment

The authors express their gratitude to K.Azekura of Energy Research Laboratory, Hitachi Ltd. for his valuable advice.

References

(1) Finnemann, H., Wagner, M.R.: Int. Meeting of specialists on Methods of Neutron Transport Theory in Reactor Calculation, Bologna, Italy, (1975)

(2) Suzuki, T.: J. Nucl. Sci. Technol., 12 [11], 695 (1975)

(3) Askew, J.R., et al.: CONF-720901, (1972)

(4) Fowler, T.B., et al.: ORNL-TM-2496, (1971)

(5) Wagner, M.R.: GA-8307, (1968)

Table 1 Three-group neutron cross sections used in calculations

Region	Energy group	$D^{\dagger}$	Σ_a	$\nu\Sigma_f$	$\Sigma_s^{g\to g+1}$	$\Sigma_s^{g\to g+2}$
Inner core	1	2.540	4.984-3††	1.235-2	2.544-2	5.625-4
	2	1.724	2.939-3	5.225-3	6.551-3	0.0
	3	1.264	7.333-3	7.684-3	0.0	0.0
Outer core	1	2.548	5.689-3	1.467-2	2.497-2	5.548-4
	2	1.725	3.534-3	6.955-3	6.341-3	0.0
	3	1.269	8.099-3	9.986-3	0.0	0.0
Blanket	1	2.173	4.304-3	8.631-3	3.288-2	7.468-4
	2	1.439	1.843-3	5.995-4	1.000-2	0.0
	3	1.026	7.611-3	1.381-3	0.0	0.0
Control rod	1	2.500	1.214-3	0.0	2.185-2	2.163-4
	2	1.681	3.348-3	0.0	9.379-3	0.0
	3	1.269	1.497-2	0.0	0.0	0.0
Sodium channel	1	4.805	1.579-4	0.0	1.130-2	6.718-5
	2	3.262	7.774-5	0.0	3.571-3	0.0
	3	2.431	3.072-4	0.0	0.0	0.0

† D : Diffusion coefficient (cm)

Σ_a : Macroscopic absorption cross section (cm^{-1})

$\nu\Sigma_f$: Macroscopic production cross section (cm^{-1})

$\Sigma_s^{g\to g'}$: Macroscopic scattering cross section from group g to g' (cm^{-1})

†† Read as 4.984×10^{-3}

Table 2 Neutron multiplication factor and control-rod-worth by three calculation methods†

Methods	K_{eff}			Control rod worth (%ΔK)	
	Pattern A	B	C	A-B	A-C
Fine mesh calculation	1.0723	1.0464	1.0224	2.59	4.99
Present coarse mesh calculation	1.0712 (-0.1)‡	1.0450 (-0.1)	1.0212 (-0.1)	2.62 (1.2)	5.00 (0.2)
Conventional coarse mesh calculation	1.0780 (0.5)	1.0555 (0.9)	1.0333 (1.1)	2.25 (-13.1)	4.47 (-10.4)

† Convergence criteria : $|\Delta K/K| \leqq 10^{-4}$ and $|\Delta\phi/\phi| \leqq 10^{-3}$

‡ Percent difference from the fine mesh calculation by CITATION code

Table 3 Power fraction by regions obtained with three calculational methods[%]

Pattern	Methods	Inner core	Outer core	Blanket
A	Fine mesh calculation	53.59	37.35	9.06
	Present coarse mesh calculation	53.79 (0.4)†	37.15 (-0.5)	9.06 (0.0)
	Conventional coarse mesh calculation	53.37 (-0.4)	37.95 (1.6)	8.68 (-4.3)
B	Fine mesh calculation	53.66	37.28	9.06
	Present coarse mesh calculation	53.85 (0.4)	37.09 (-0.5)	9.06 (0.0)
	Conventional coarse mesh calculation	53.41 (-0.5)	37.92 (1.7)	8.67 (-4.3)
C	Fine mesh calculation	53.64	37.12	9.24
	Present coarse mesh calculation	53.85 (0.4)	36.91 (-0.6)	9.24 (0.0)
	Conventional coarse mesh calculation	53.39 (-0.5)	37.79 (1.8)	8.82 (-4.5)

† Percent difference in power fraction relative to fine mesh calculation

Table 4 Computing time for three calculational methods

Methods	CPU time (sec)†		
	Pattern A	B	C
Fine mesh calculation	4097	4668	4934
Present coarse mesh calculation	473	556	497
Conventional coarse mesh calculation	319	352	351

† Time required for diffusion calculations performed on ACOS-6/S800

List of Figure

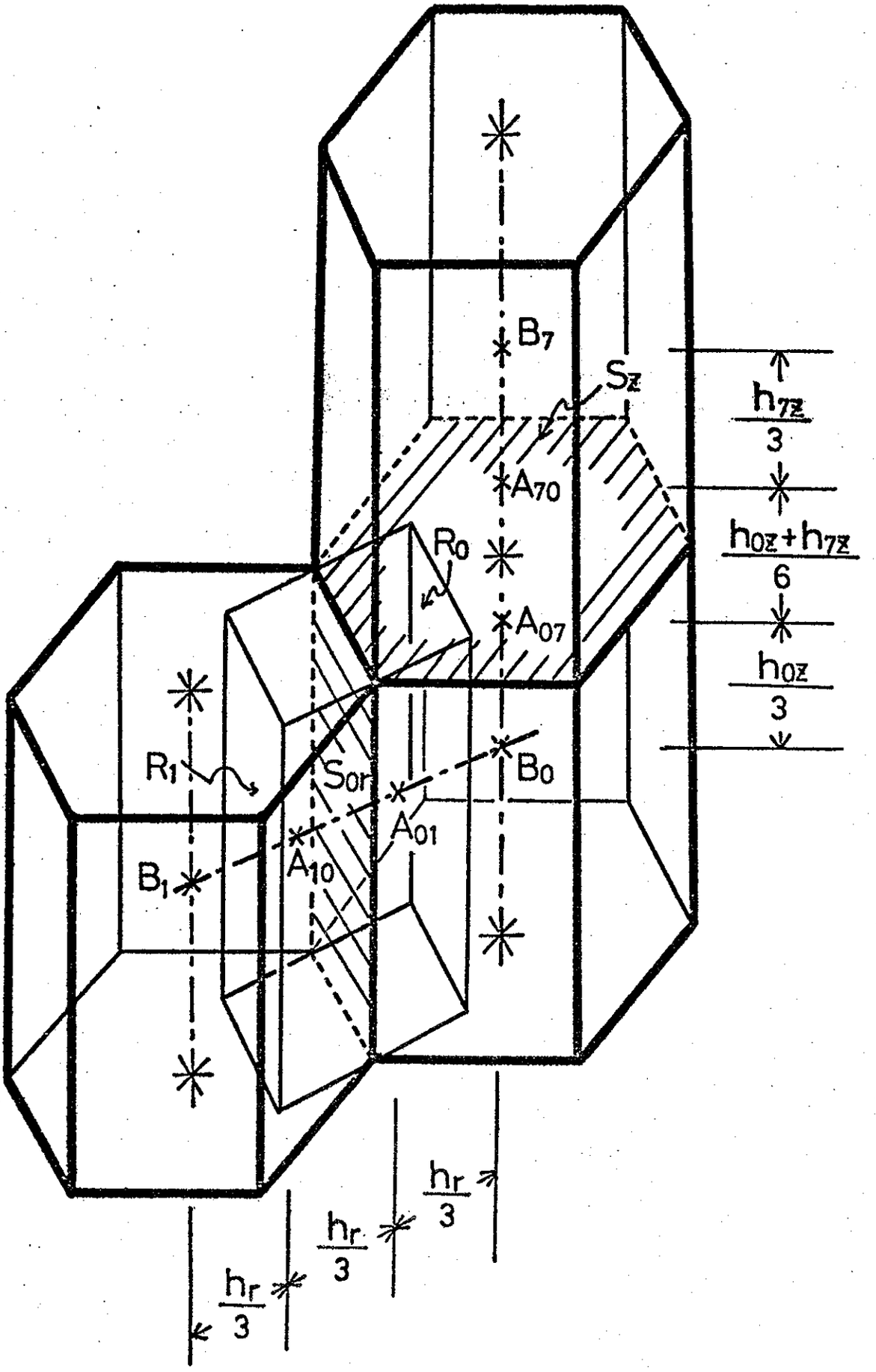

Fig. 1 Mesh points for calculating neutron balances in 3-D geometry

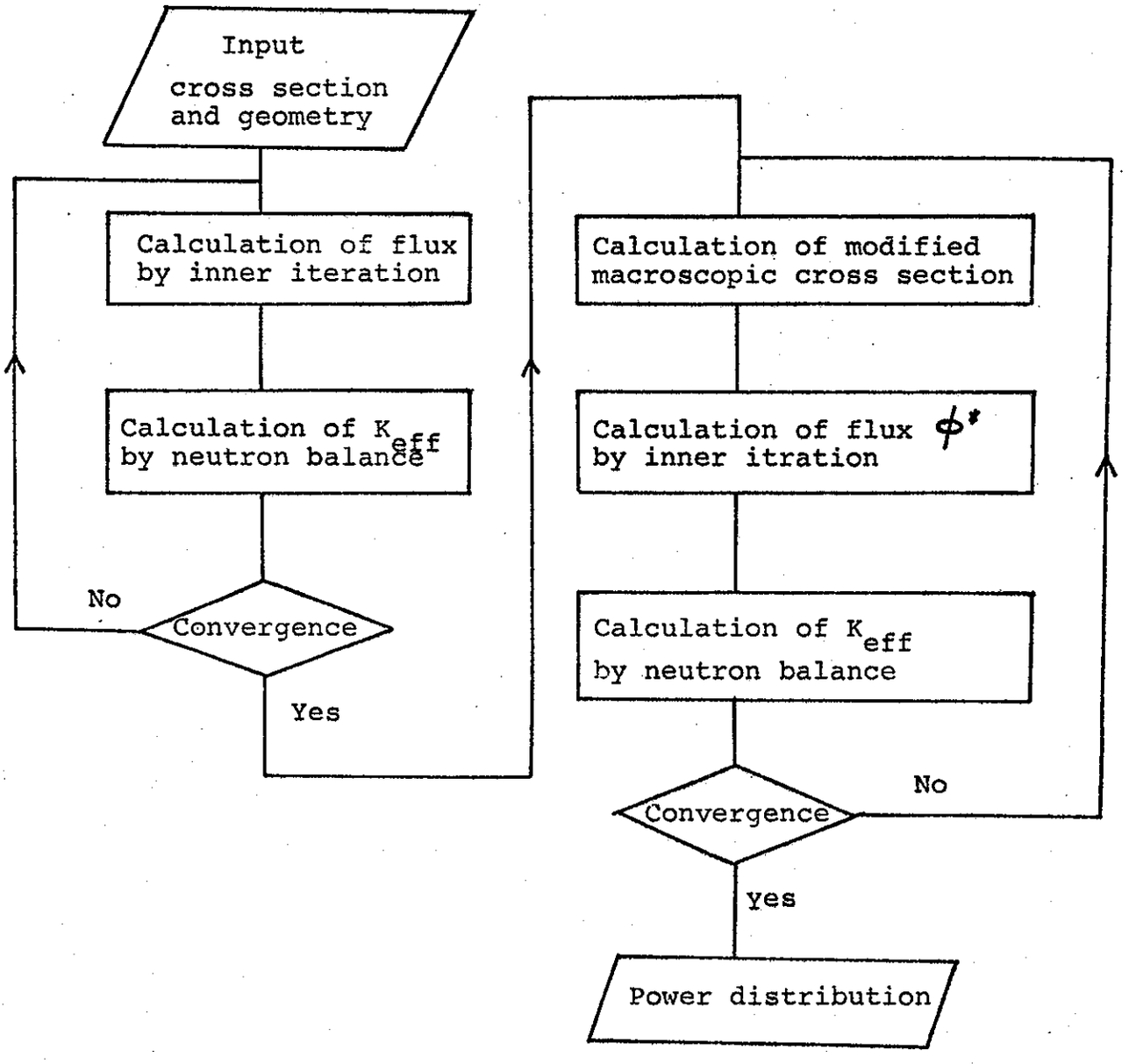

Fig. 2 Calculational flow of the improved coarse mesh method

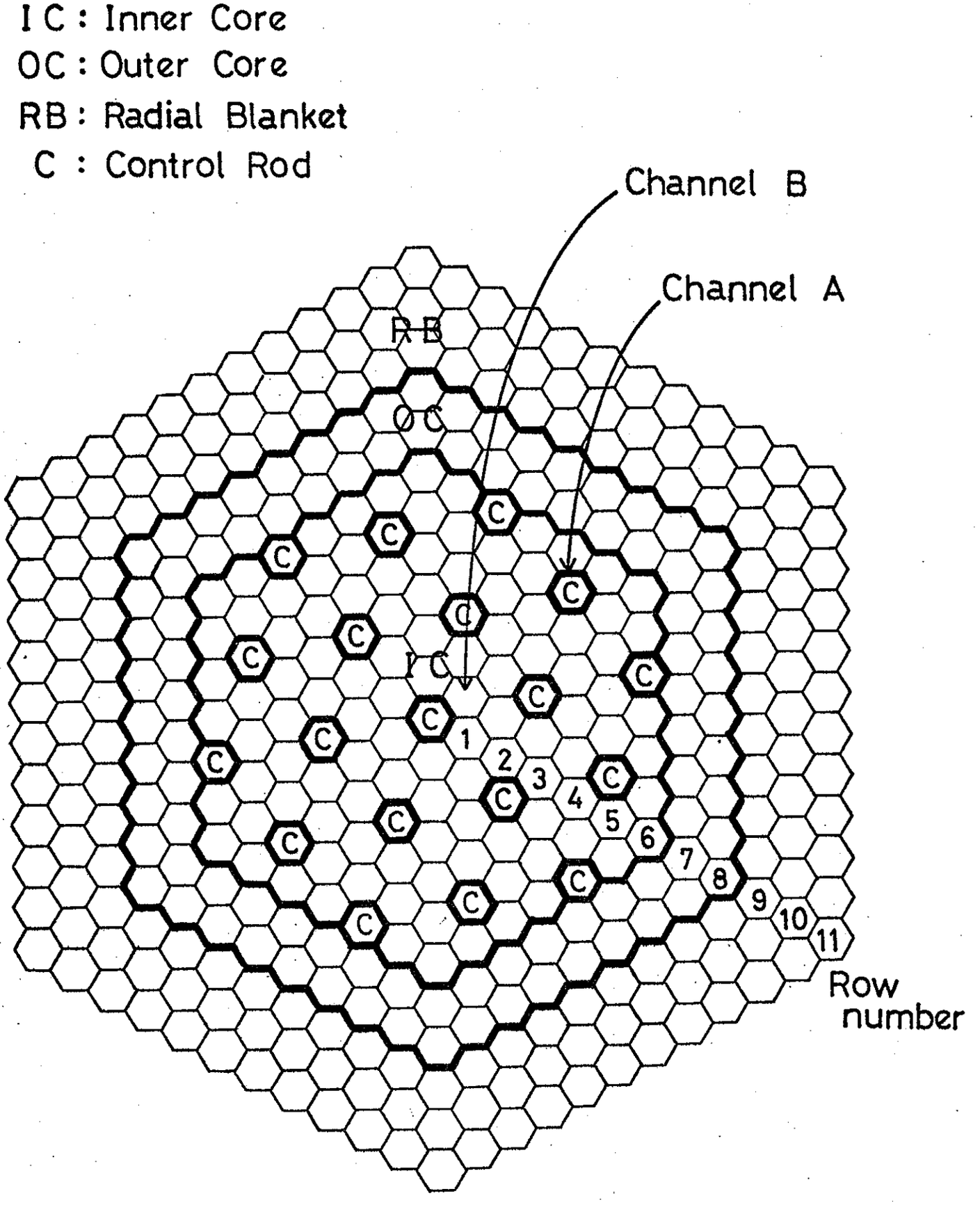

Fig. 3 Cross-sectional view of the core used for test calculations

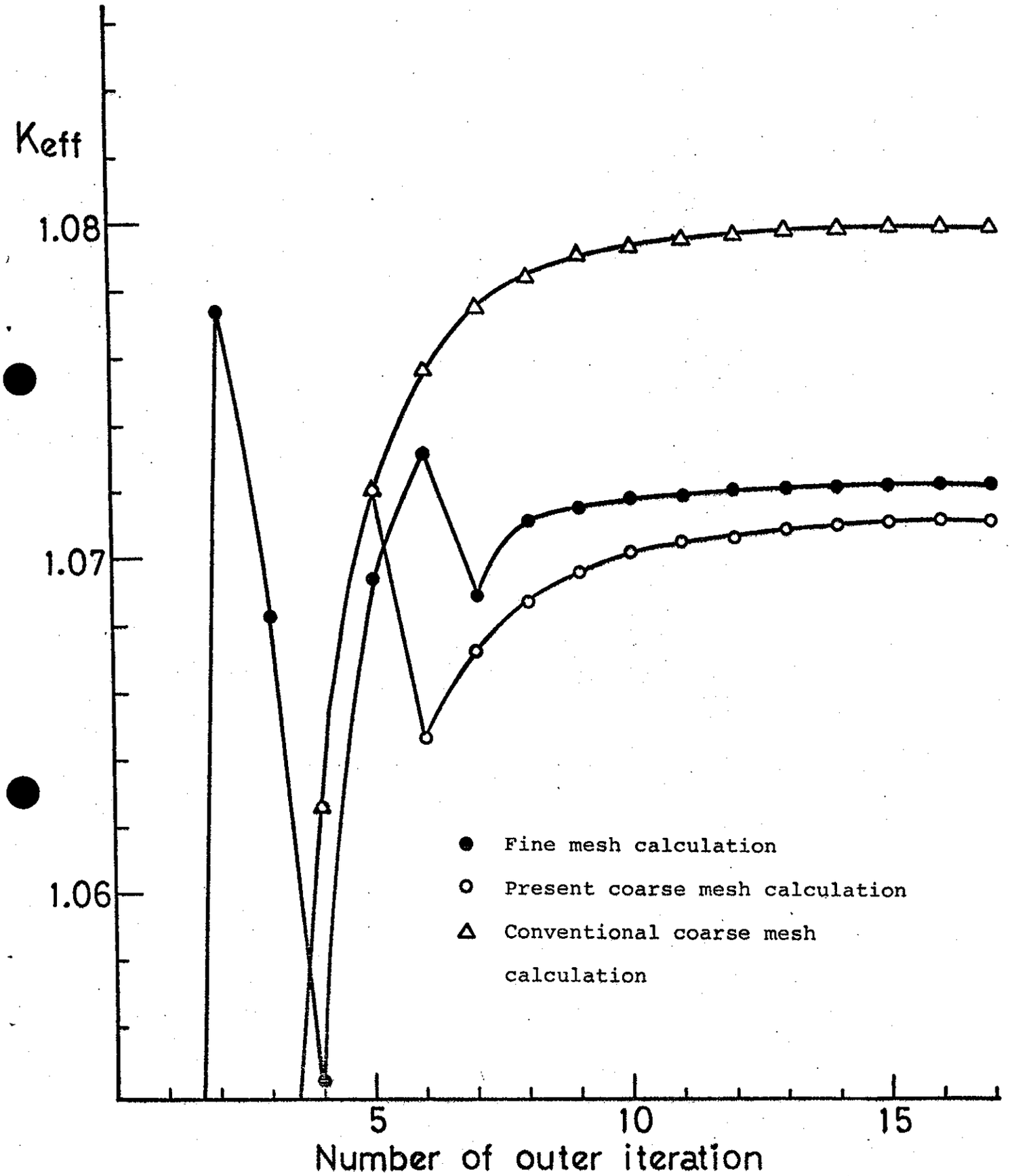

Fig. 4(a) Convergence of neutron multiplication factor as a function of number of outer iterations for the pattern A

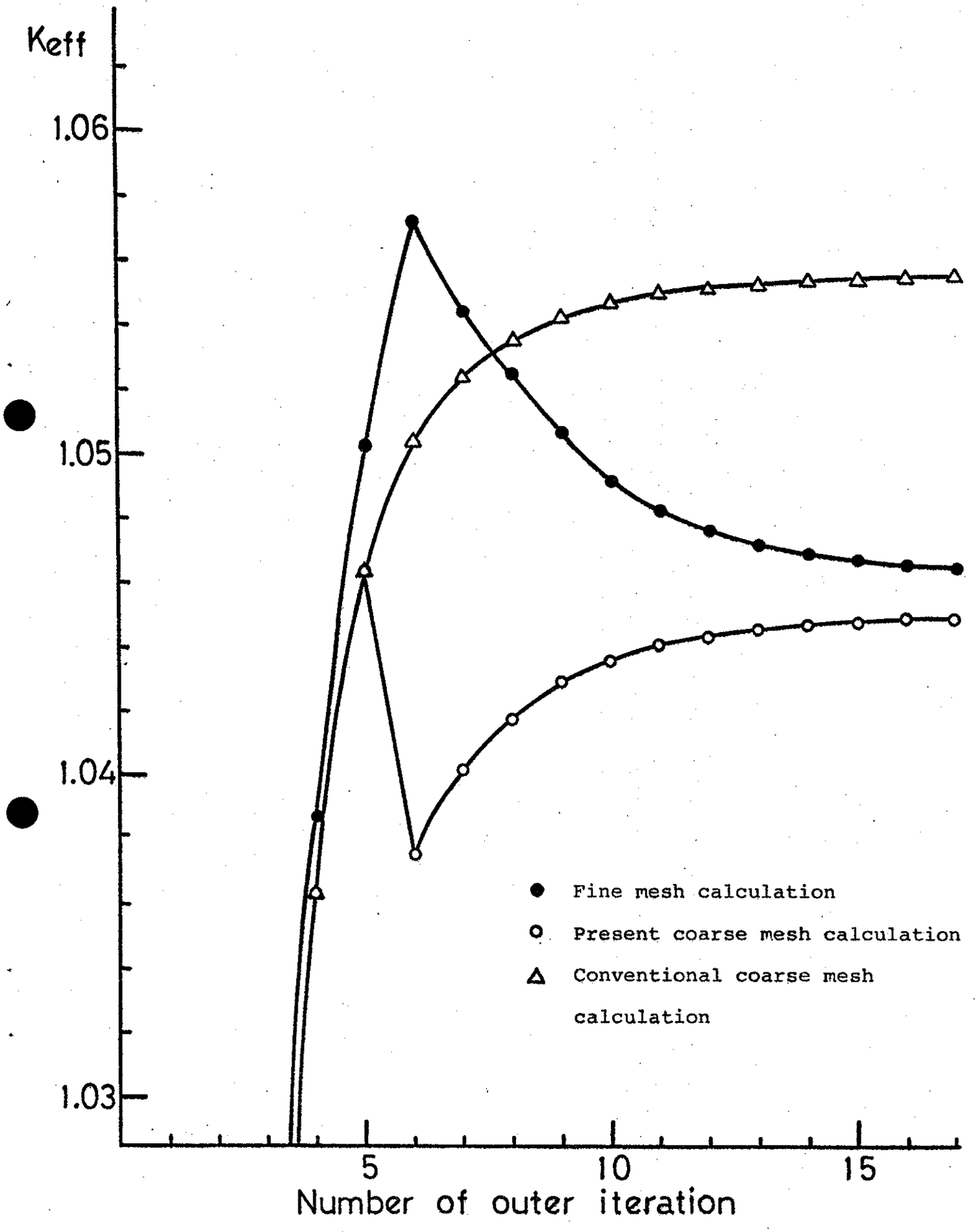

Fig. 4(b) Convergence of neutron multiplication factor as a function of number of outer iterations for the pattern B

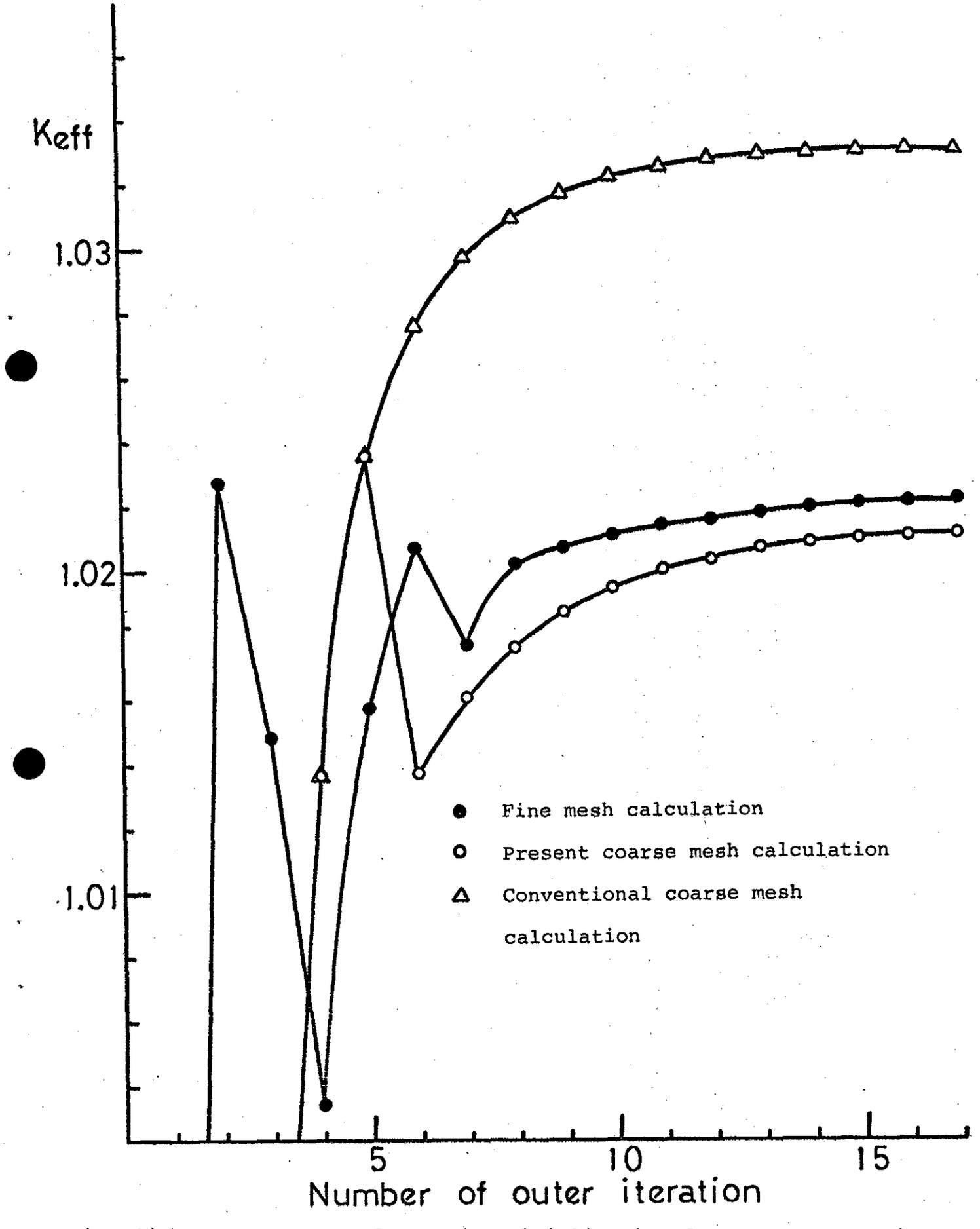

Fig. 4(c) Convergence of neutron multiplication factor as a function of number of outer iterations for the pattern C

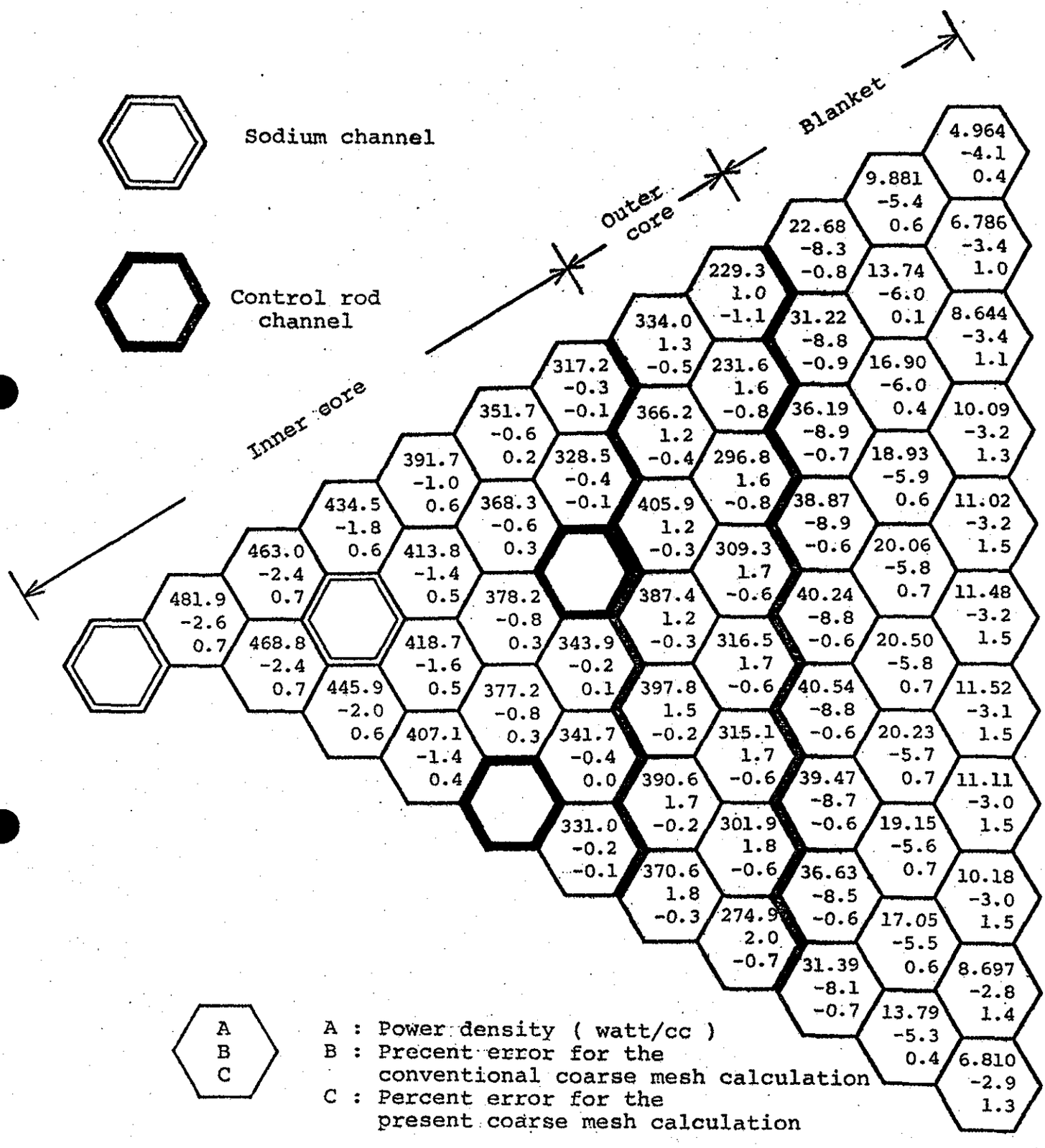

Fig. 5(a). Power density and percent error in power density for the conventional and the present coarse mesh calculations for the pattern B on a central radial plane

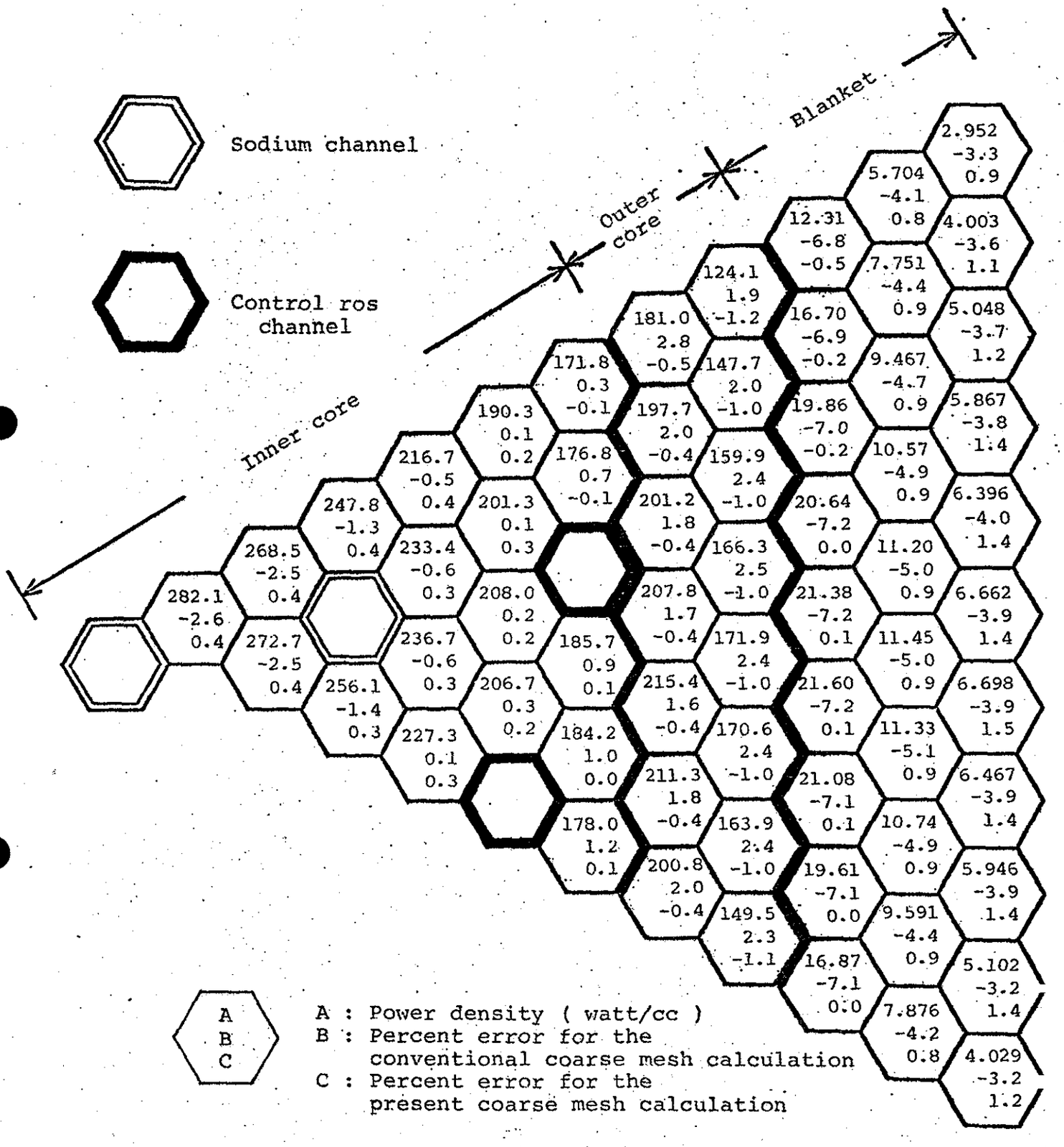

Fig. 5(b) Power density and percent error in power density for the conventional and the present coarse mesh calculations for the pattern B on a radial plane adjacent to upper blanket

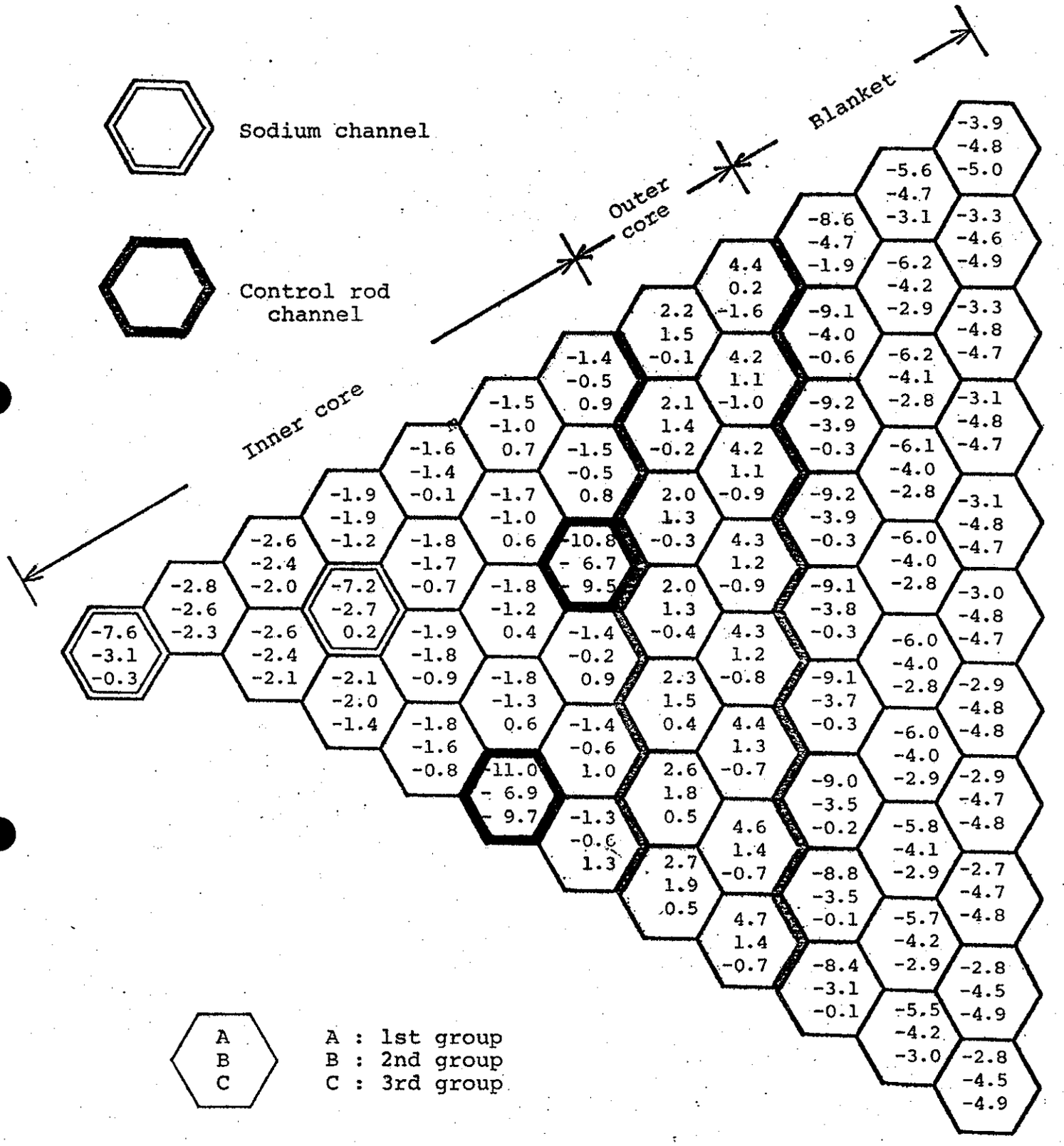

Fig. 6(a) Percent errors in each of the three-group fluxes on a central plane for the pattern B for the conventional coarse mesh calculation

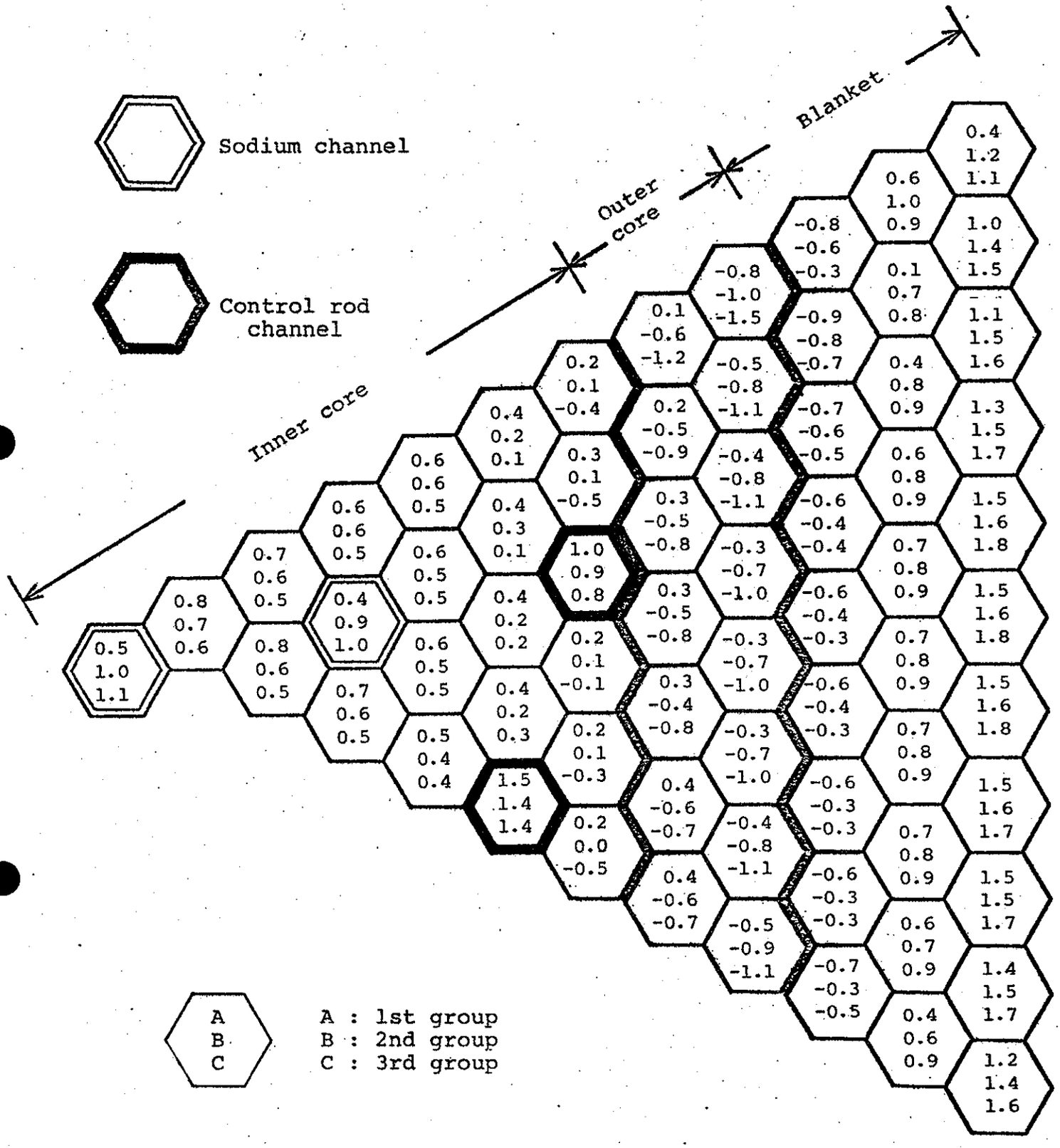

Fig. 6(b) Percent errors in each of the three-group fluxes on a central plane for the pattern B for the present coarse mesh calculation

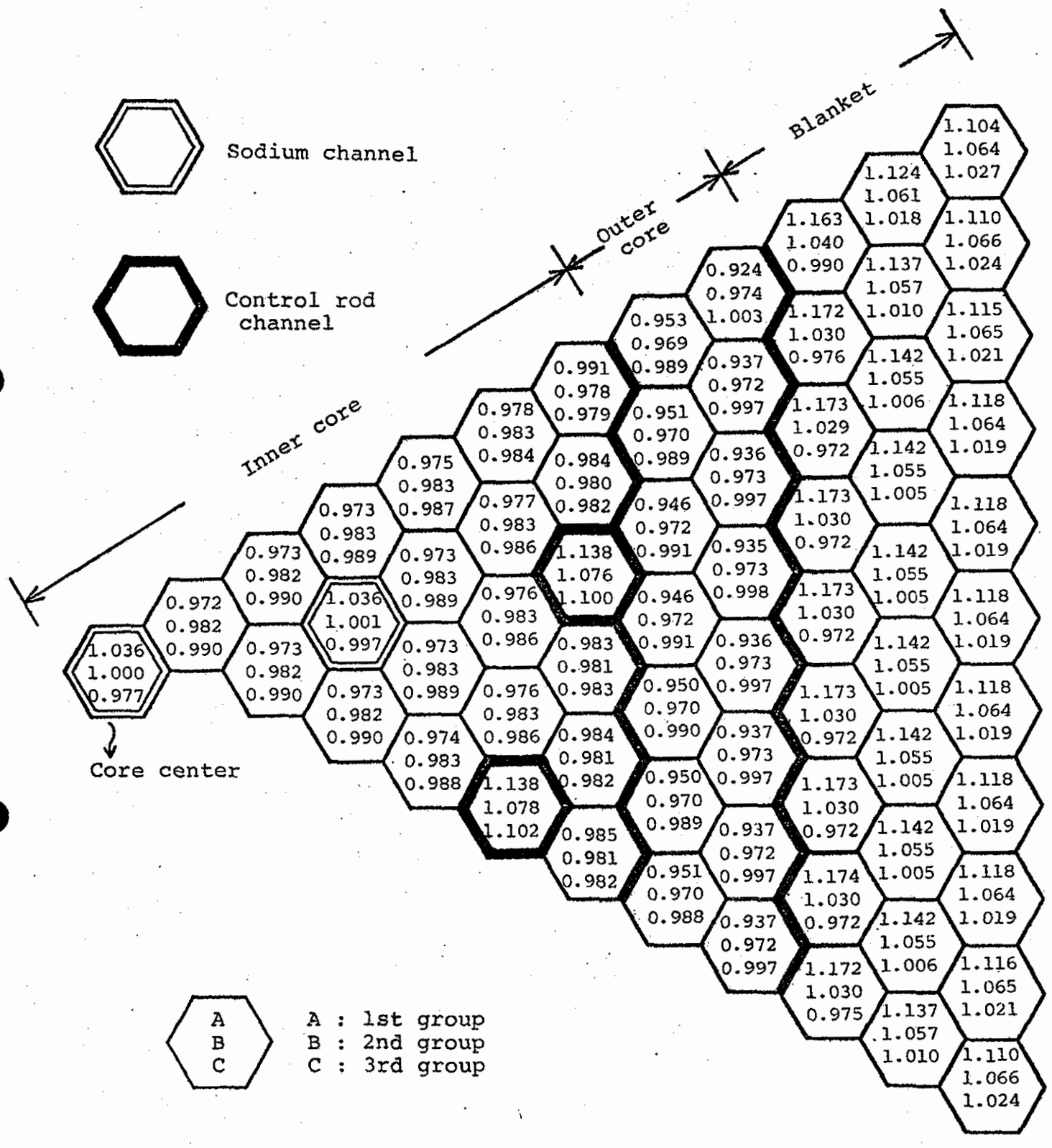

Fig. 7 Correction factors for three-group macroscopic cross sections on a central plane used in improved coarse mesh calculation for the pattern B

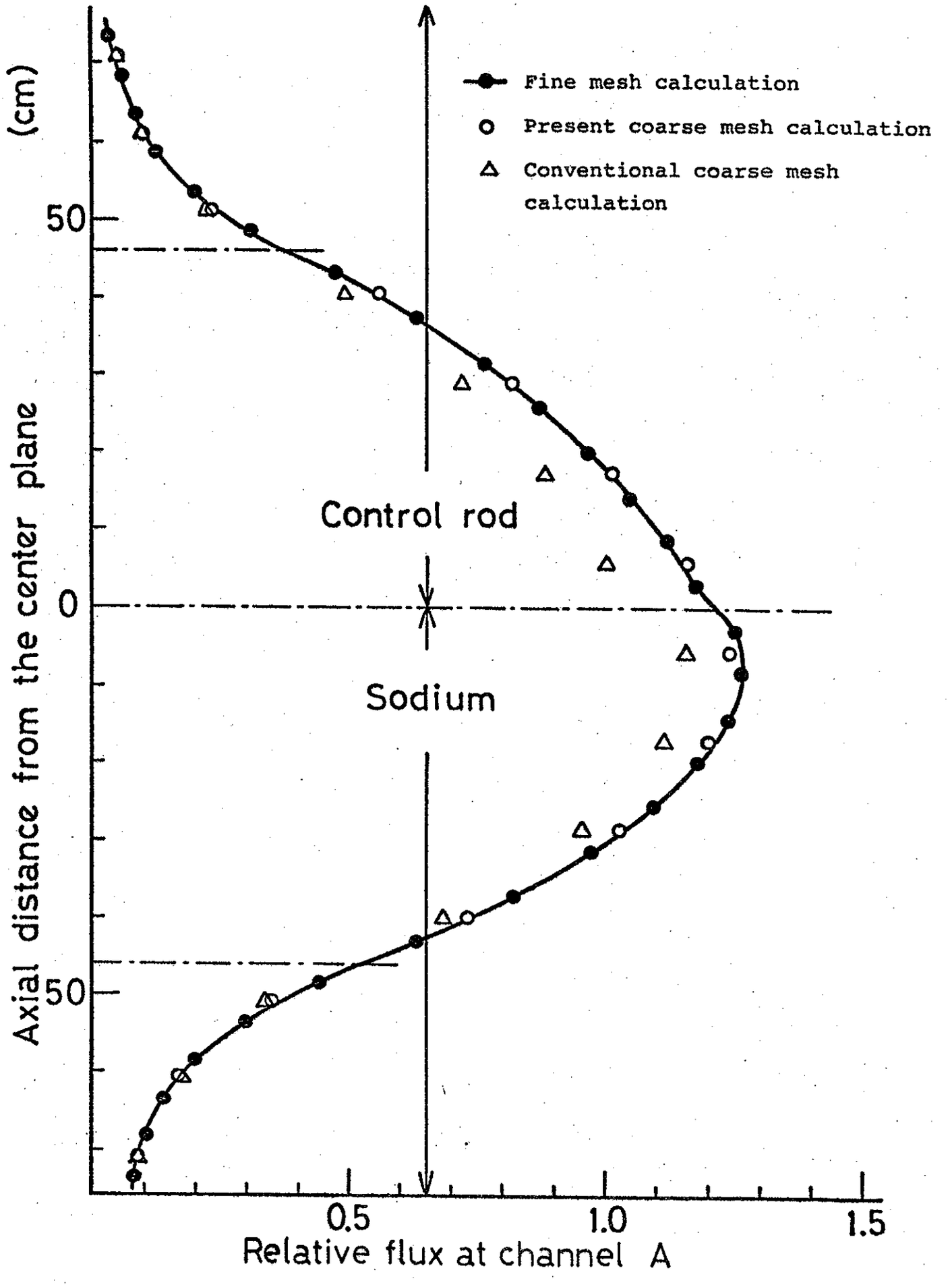

Fig. 8(a) 1st-group axial flux distribution at the control-rod channel for the pattern R

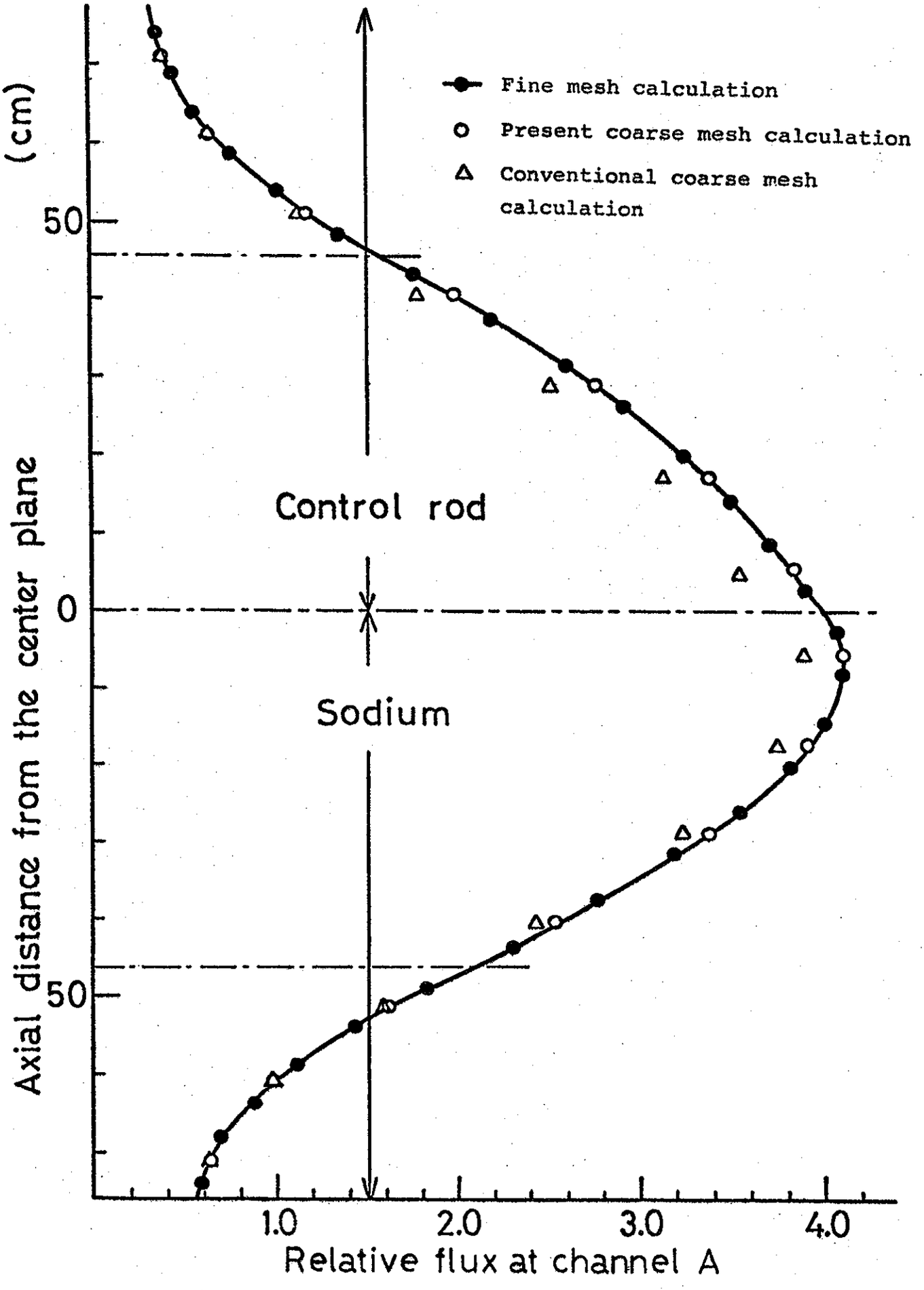

Fig. 8(b) 2nd-group axial flux distribution at the control-rod channel for the pattern B

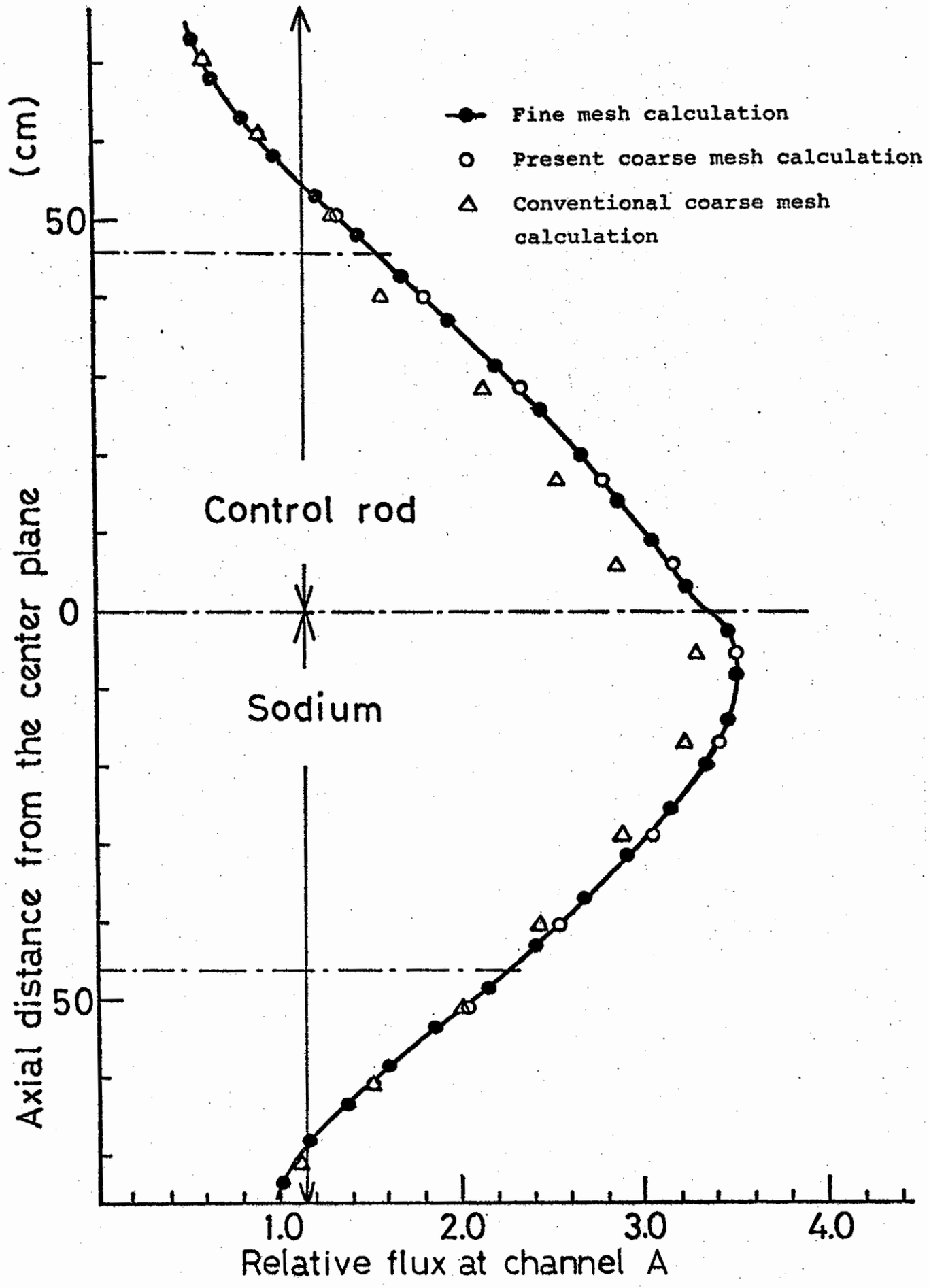

Fig. 8(c) 3rd-group axial flux distribution at the control-rod channel for the pattern B

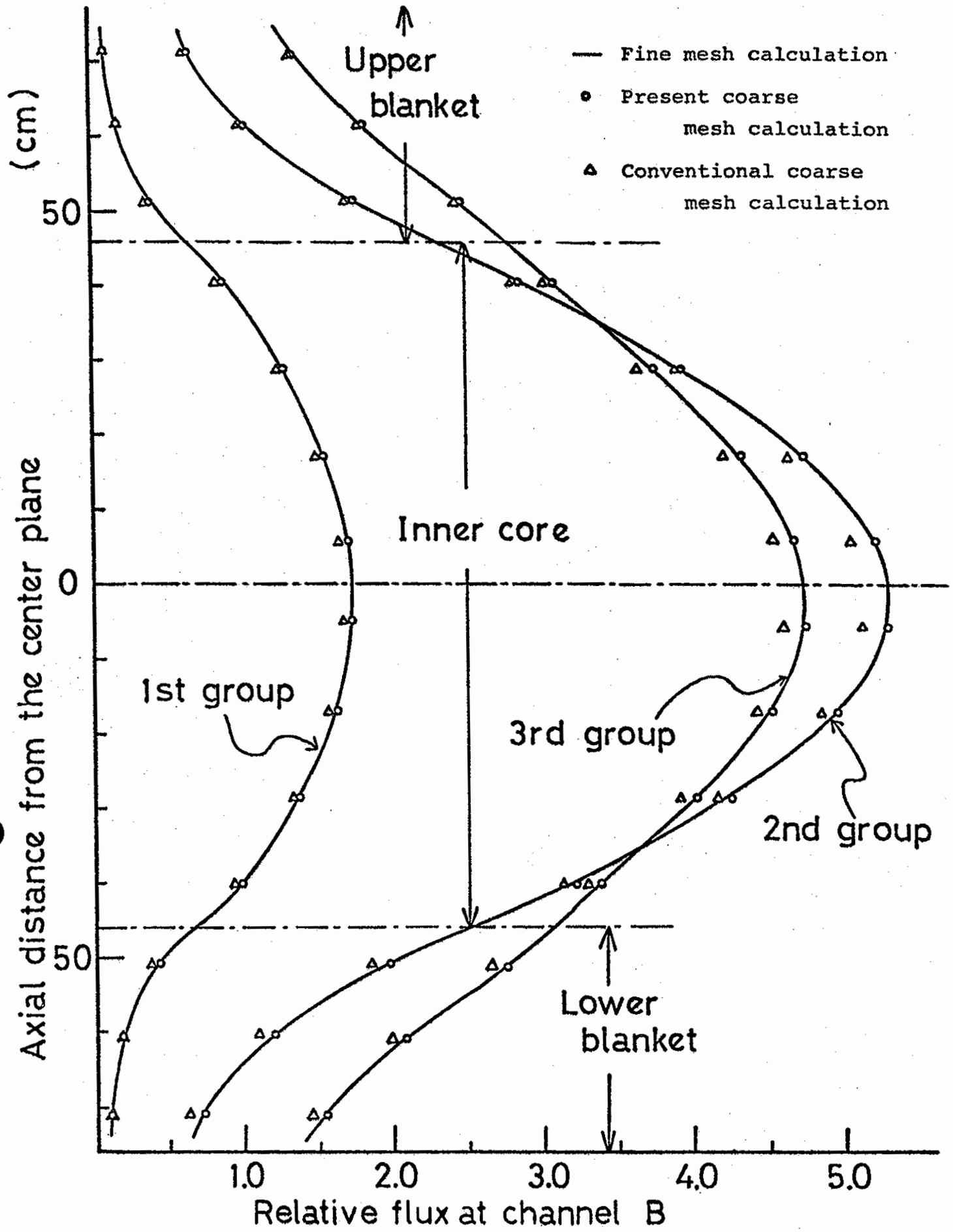

Fig. 9 The axial group-flux distributions along the fuel assembly at the core center for the pattern B